NANO LETTERS

pubs.acs.org/NanoLett Letter

Tunneling Spectroscopy in Carbon Nanotube-Hexagonal Boron Nitride-Carbon Nanotube Heterojunctions

Sihan Zhao,*▲ SeokJae Yoo,▲ Sheng Wang,▲ Bosai Lyu, Salman Kahn, Fanqi Wu, Zhiyuan Zhao, Dingzhou Cui, Wenyu Zhao, Yoseob Yoon, M. Iqbal Bakti Utama, Wu Shi, Kenji Watanabe, Takashi Taniguchi, Michael F. Crommie, Zhiwen Shi, Chongwu Zhou, and Feng Wang*

Cite This: *Nano Lett.* 2020, 20, 6712−6718 Read Online

ACCESS | Metrics & More | Article Recommendations | Supporting Information

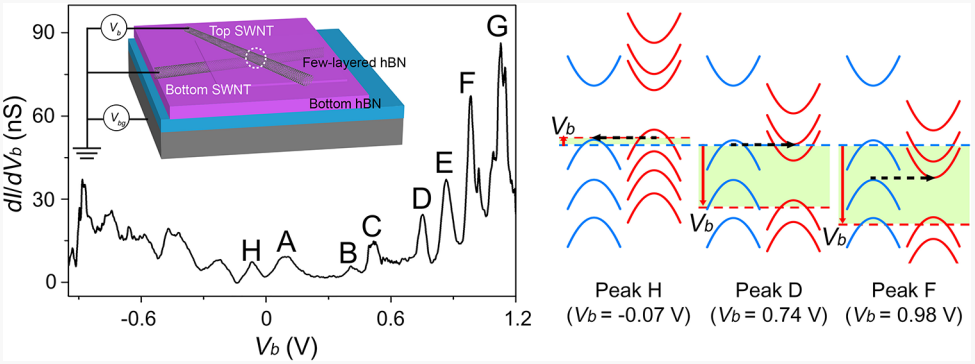

ABSTRACT: Electron tunneling spectroscopy is a powerful technique to probe the unique physical properties of one-dimensional (1D) single-walled carbon nanotubes (SWNTs), such as the van Hove singularities in the density of states or the power-law tunneling probability of a Luttinger liquid. However, little is known about the tunneling behavior between two 1D SWNTs over a large energy spectrum. Here, we investigate the electron tunneling behavior between two crossed SWNTs across a wide spectral window up to 2 eV in the unique carbon nanotube-hexagonal boron nitride-carbon nanotube heterojunctions. We observe many sharp resonances in the differential tunneling conductance at different bias voltages applied between the SWNTs. These resonances can be attributed to elastic tunneling into the van Hove singularities of different 1D subbands in both SWNTs, and they allow us to determine the quasi-particle bandgaps and higher-lying 1D subbands in SWNTs on the insulating substrate.

KEYWORDS: *band-to-band tunneling, tunneling spectroscopy, mixed dimensions, heterojunctions, carbon nanotubes, hexagonal boron nitride*

Electrons confined in one-dimension (1D) show distinct behavior from their higher-dimensional counterparts. They exhibit divergence in the density of states (DOS) known as a van Hove singularity, and these confined electrons form a strongly correlated system described by a Luttinger liquid which exhibits a unique power-law decay of correlation functions and spin-charge separation.[1−5] Electron tunneling spectroscopy is a powerful tool to characterize the unique 1D physics in systems such as single-walled carbon nanotubes (SWNTs). Previously, for example, scanning tunneling microscopy (STM) enabled the first observation of the van Hove singularity in individual SWNTs.[6−8] Typical limitations of STM are the requirement for the nanotubes to be on a conductive substrate and the difficulty in studying electron tunneling between two 1D objects. Electrical transport measurements have been used to study electron tunneling between the metal contact and SWNTs and between crossed SWNTs, which revealed signatures of Luttinger liquid physics.[9−12] These studies, however, have been limited to a very narrow spectral window (∼100 meV) due to the lack of a well-defined tunneling barrier, which prohibits the experimental exploration of electron tunneling under a strong non-equilibrium condition.

In this Letter, we report the tunneling spectroscopy between two SWNTs over a large spectral window of ∼2 eV using a unique carbon nanotube-hexagonal boron nitride-carbon nanotube heterojunction. Hexagonal boron nitride (hBN) is an insulating two-dimensional (2D) material with a large bandgap and high breakdown electric field.[13,14] The hBN layer

Received: June 21, 2020
Revised: August 3, 2020
Published: August 4, 2020

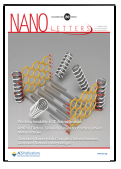

https://dx.doi.org/10.1021/acs.nanolett.0c02585
Nano Lett. 2020, 20, 6712−6718

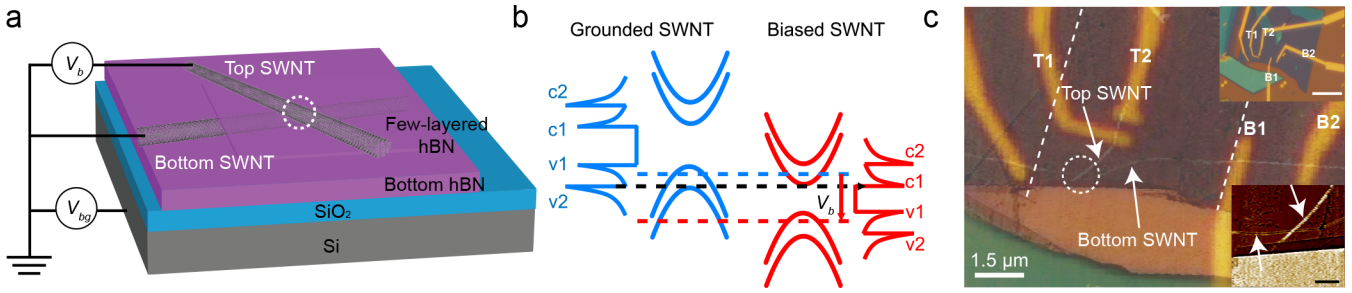

Figure 1. Device structure for tunneling spectroscopy in a 1D heterojunction. (a) Schematic drawing of the 1D heterojuntion device for the electron tunneling measurement. Two crossed SWNTs are separated by the few-layered hBN forming a point tunneling junction (dashed circle). A bias voltage V_b and a global backgate voltage V_{bg} can be applied. (b) Schematic illustration of the control of band alignments and the band-to-band tunneling process with the applied V_b. The solid blue and red parabolic lines represent the band structures of the grounded and biased semiconducting SWNTs, respectively. The associated 1D DOS are plotted at the sides of the band structures with *vi* and *ci* (i = 1, 2, 3, etc.) denoting the van Hove singularity position in the valence and conduction subbands. The dashed blue and red lines denote the Fermi energies in the two hole-doped semiconducting SWNTs. The schematic illustrates a band-to-band resonant tunneling process when v2 of the grounded SWNT aligns with c1 of the biased SWNT (dashed black arrow) inside an energy window set by the two Fermi energies. (c) Optical image of a typical tunneling device with an AFM image overlaid. The top and bottom SWNTs are indicated by the white arrows. Electrodes T1 and T2 are contacts for the top SWNT, and B1 and B2 are contacts for the bottom SWNT. The straight dashed lines show the boundaries of the few-layered hBN tunneling barrier. The tunneling junction formed between two crossed SWNTs is indicated by the dashed circle. The inset of Figure 1c (bottom right) shows an enlarged view of the tunneling junction with the top and bottom SWNTs indicated by the white arrows; the scale bar is 500 nm. The inset of Figure 1c (upper right) shows an enlarged view of the device; the scale bar is 10 μm. Tunneling conductance of the junction can be measured between contacts T1 and B1 as a function of V_b and V_{bg}, while the conductance of each individual SWNT can be monitored through contacts T1, T2 and B1, B2.

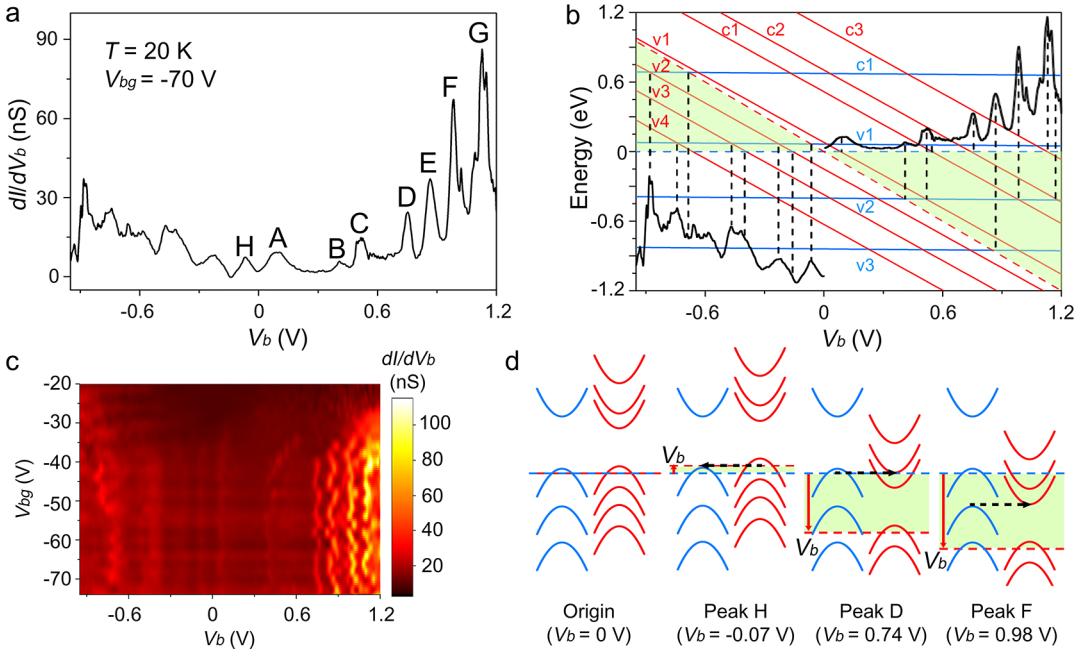

Figure 2. Tunneling spectroscopy of a semiconducting/semiconducting SWNT heterojunction. (a) Differential conductance dI/dV_b measured at the backgate voltage V_{bg} = −70 V at 20 K. The data is obtained while the bottom SWNT is grounded and the top SWNT is biased as shown in Figure 1a. The representative elastic band-to-band tunneling peaks associated with the van Hove singularities of 1D subbands in two SWNTs are denoted as A, B, C, and so forth. (b) Analysis of the tunneling spectrum of (a). The solid blue and red lines represent the van Hove singularity positions in subbands (*vi* and *ci*) of the grounded bottom SWNT and the biased top SWNT as V_b changes, respectively. The dashed blue and red lines denote the Fermi energies in the two hole-doped SWNTs. The energy window allowing for the electron tunneling to happen is indicated by the shaded green region. Each crossing of the blue (or dashed blue) line with the red (or dashed red) line within the shaded green region gives rises to a dI/dV_b peak that is indicated by the dashed black line. The slopes of the red and blue lines in Figure 2b are close to −1 and 0 for the biased top SWNT and grounded bottom SWNT, respectively, indicating a small band shift as V_b changes. (c) The 2D differential conductance map as a function of V_b and V_{bg} at 20 K, showing a weak dependence of dI/dV_b spectra on the backgate voltages. (d) Illustration of the band alignments at four representative bias voltages: V_b = 0 V (origin), V_b = −0.07 V (peak H), V_b = 0.74 V (peak D), and V_b = 0.98 V (peak F). The band alignments shown in (d) are determined from the analysis result of (b). The solid blue and red parabolic lines represent the band structures of the grounded and biased SWNTs. The elastic band-to-band tunneling processes giving rise to peaks H, D, and F are indicated by the dashed black arrows. The energy window for the tunneling is also indicated by the shaded green region.

https://dx.doi.org/10.1021/acs.nanolett.0c02585
Nano Lett. 2020, 20, 6712−6718

provides an excellent tunneling barrier in heterostructure devices, as recently demonstrated in a variety of 2D van der Waals heterostructures.[15−19] We measure the tunneling current of the point tunneling junction between two crossed semiconducting SWNTs as a function of the bias voltage (V_b) and the backgate voltage (V_{bg}) at low temperature. We observe multiple sharp peaks in the differential conductance (dI/dV_b) at different V_b. These peaks can be mostly attributed to elastic resonant tunneling when the energy of the van Hove singularity in one SWNT aligns with either the Fermi energy or the van Hove singularity in the other SWNT.[20] The measured tunneling spectroscopy in the 1D heterojunction allows us to determine the quasi-particle bandgaps and positions of higher-lying subbands in the two constituent SWNTs. Band-to-band tunneling is also observed in a heterojunction composed of a semiconducting and a metallic SWNT.

RESULTS AND DISCUSSION

The tunneling device was prepared by a dry-transfer technique similar to that developed in fabricating 2D van der Waals heterostructures (Methods).[21] In brief, the top SWNT, few-layered hBN (two or three layers Figure S1), and the bottom SWNT grown on top of a large bottom hBN substrate were sequentially picked up and finally deposited on a fresh SiO_2/Si substrate with 285 nm oxide thickness by a polycarbonate (PC) dry-transfer technique.[22] Figure 1a shows the schematic illustration of our device structure, where the two crossed SWNTs separated by few-layered hBN form a point tunneling junction (dashed circle). A global backgate voltage (V_{bg}) is applied to change carrier densities in both SWNTs. A bias voltage (V_b) is applied to the top SWNT while the bottom SWNT is grounded as schematically shown in Figure 1a. If the resistance of the tunneling junction dominates, the applied V_b drops mostly across the hBN tunneling barrier, which enables us to effectively tune the relative band alignments of two SWNTs over a large energy spectrum. Figure 1b schematically illustrates the control of the band alignment of the two SWNTs with V_b when two individual semiconducting SWNTs are hole-doped. We denote the van Hove singularity position of the valence and conduction subbands in SWNTs as v*i* and c*i* throughout this paper, where *i* represents the *i*th valence or conduction subbands with i = 1, 2, 3, and so forth. A representative band-to-band resonant tunneling process is illustrated in Figure 1b, in which c1 of the biased SWNT aligns with v2 of the grounded SWNT (dashed black arrow). The optical image of a typical device structure is shown in Figure 1c with an atomic force microscopy (AFM) image overlaid. The straight dashed lines delineate the boundaries of the few-layered hBN tunneling barrier (not optically visible), and the dashed circle indicates the location of the tunneling junction. The inset of Figure 1c (bottom right) shows an enlarged view of the tunneling junction. Electrodes contacting the top (bottom) SWNT are made of Pd/Au (10 nm/75 nm) and are denoted as T1 (B1) and T2 (B2) in Figure 1c (Supporting Information Note 1). We can measure the tunneling conductance of the heterojunction through the probes T1 and B1, whereas the transport properties of individual top and bottom SWNTs can be independently monitored through T1, T2 and B1, B2, respectively (Supporting Information Note 1). The inset of Figure 1c (upper right) shows an enlarged view of the device.

Figure 2a presents the differential conductance dI/dV_b of a tunneling junction composed of two crossed semiconducting SWNTs; the data is obtained at 20 K while biasing the top SWNT and grounding the bottom SWNT. We characterize the diameters of the top and bottom semiconducting SWNTs with AFM and determine their diameters to be about 2.2 and 1.6 nm, respectively (Figure S2). We note that the AFM determination of the top SWNTs was carried out after the sample transfer, which may result in some uncertainty due to the residues. The gate-dependent measurement at near zero-bias condition at 20 K for each individual SWNT is shown in Figure S3. The data in Figure 2a is obtained at $V_{bg} = -70$ V, where both semiconducting SWNTs are hole-doped with a two-terminal conductance of ∼1 and ∼10 μS (Figure S3). This single-tube conductance is more than 1 order of magnitude higher than that of the tunneling junction. Therefore, most of V_b drops across the hBN tunneling junction between two SWNTs. We observe many prominent dI/dV_b peaks in the tunneling spectrum in Figure 2a. A consistent tunneling spectrum is observed in Figure S4 when reversing the grounding condition. The temperature-dependent DC current as a function of V_b obtained at $V_{bg} = -70$ V is shown in Figure S5.

We can understand the tunneling spectrum in Figure 2a based on elastic tunneling between the SWNTs, where the peaks arise from the van Hove singularities in the DOS of 1D subbands. The total tunneling current at low temperature (that is neglecting the thermal excitation) is proportional to the convolution of DOS in two SWNTs over an energy window set by the applied bias voltage V_b as follows

$$I(V_b) = \frac{2\pi e}{\hbar}|M|^2 \int_0^{-eV_b} D_1(\varepsilon + E_{F1} - E_{i1} + eV_b) D_2 (\varepsilon + E_{F2} - E_{i2}) d\varepsilon \quad (1)$$

where $D_1(\varepsilon)$ and $D_2(\varepsilon)$ are the 1D DOS for the biased and grounded SWNTs referenced to their intrinsic Fermi energies E_{i1} and E_{i2} in the two SWNTs, that is to say, $D_1(0)$ and $D_2(0)$ are the corresponding DOS at the middle of the bandgaps. e and $\hbar$ represent the elementary charge and reduced Planck constant, E_{F1} and E_{F2} denote the Fermi energies of the biased and grounded SWNTs, and the transition matrix element M is assumed to be a constant over a finite energy.[23,24] Elastic resonant tunneling occurs when the energy of the van Hove singularities in one SWNT aligns with either the Fermi energy or the van Hove singularities in the other SWNT within the bias window (i.e., Fermi energies of two SWNTs).

Figure 2b shows the analysis of the measured spectrum (Figure 2a). The horizontal axis is the applied V_b, and the vertical axis is the energy in electronvolts. The Fermi energy of the grounded bottom SWNT (E_{F2}) is fixed to zero (dashed blue line) and that of the biased top SWNT (E_{F1}) moves with V_b (dashed red line). The positions of v*i* and c*i* for the grounded bottom SWNT and the biased top SWNT at the heterojunction as a function of V_b are shown as the solid blue and solid red lines in Figure 2b, respectively.

We start at $V_b = 0$ V where $E_{F1} = E_{F2} = 0$ eV in the two SWNTs and both Fermi energies locate in between their own v1 and v2 (i.e., hole doping). The first dI/dV_b peak near the origin at the positive side (A peak in Figure 2a) appears at V_b = 0.10 V, which corresponds to the resonant tunneling process when E_{F2} aligns with v1 of the biased top SWNT (crossing of E_{F2} and v1 in red in Figure 2b). The first dI/dV_b peak near the

https://dx.doi.org/10.1021/acs.nanolett.0c02585
Nano Lett. 2020, 20, 6712−6718

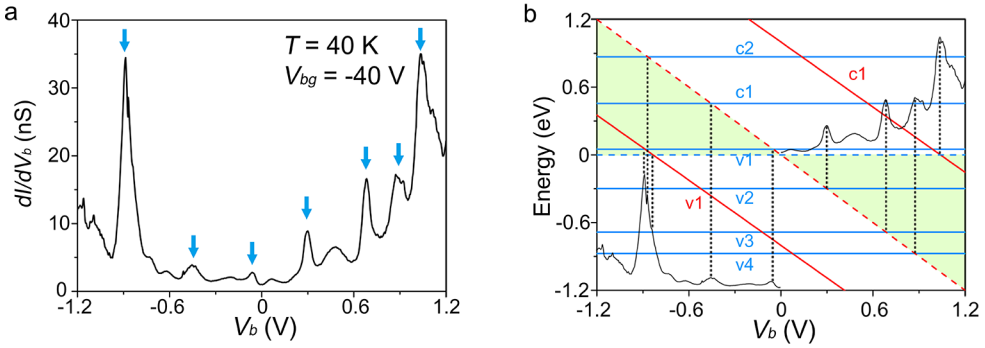

Figure 3. Tunneling spectroscopy of a semiconducting/metallic SWNT heterojunction. (a) Differential conductance dI/dV_b measured at V_{bg} = −40 V at 40 K. The data is obtained while the top semiconducting SWNT is grounded and the bottom metallic SWNT is biased. dI/dV_b peaks indicated by the blue arrows are assigned to the elastic band-to-band tunneling associated with tunneling into the van Hove singularities in two SWNTs. Other weaker and broader spectral features are assigned to the inelastic tunneling process in attendance with the strong elastic tunneling peaks. (b) Analysis of the tunneling spectrum of (a). It shows the *vi* and *ci* positions of the grounded semiconducting SWNT (solid blue lines) and the biased metallic SWNT (solid red lines) as V_b changes. The Fermi energies of the grounded semiconducting SWNT and the biased metallic SWNT are indicated by the dashed blue and dashed red lines. The energy window for the electron tunneling is indicated by the shaded green region. Each crossing of the blue (or dashed blue) line with the red (or dashed red) line within the shaded green region gives rises to a dI/dV_b peak that is indicated by the dashed black line.

origin at the negative side (H peak in Figure 2a) appears at V_b = −0.07 V, which arises when E_{F1} aligns with v1 of the grounded bottom SWNT (crossing of E_{F1} and v1 in blue in Figure 2b). As V_b increases at the positive side, the sequential energy alignments of E_{F1} with v2 of the bottom SWNT and v1 of the top SWNT with v2 of the bottom SWNT yield peaks B (V_b = 0.41 V) and C (V_b = 0.52 V) in Figure 2a. At this point, c1 of the top SWNT also approaches E_{F2}, which contributes to the formation of peak C. With more positive bias, c2 of the top SWNT makes an energy crossing with E_{F2} and that E_{F1} aligns with v3 of the bottom SWNT, which give rise to the D (V_b = 0.74 V) and E peaks (V_b = 0.87 V), respectively. Further applied positive V_b yields the peaks F and G whose origins are assigned and indicated as well by the dashed black lines in Figure 2b. Likewise, most of the main spectral features at the negative V_b side can be addressed reasonably well as shown in Figure 2b.

Figure 2c displays the 2D differential conductance map as a function of both V_b and V_{bg} at 20 K, where the dI/dV_b spectra show a weak dependence on V_{bg} for all the backgate voltages more negative than −40 V. When V_{bg} is more positive than −40 V, the dI/dV_b spectra in the 2D map diminish at small V_b and show a diverging behavior at larger V_b, which is correlated well with the low conductivity of the bottom SWNT (Figure S3). Figure 2d presents the representative band alignments at the origin (V_b = 0 V), the peak H (V_b = −0.07 V), the peak D (V_b = 0.74 V), and the peak F (V_b = 0.98 V) which are directly obtained from the analyzed result in Figure 2b.

Our analysis yields a determination of the single-particle band structure of the two constituent SWNTs. We can determine the quasi-particle bandgaps of the top and bottom SWNTs to be ∼0.44 and ∼0.61 eV, respectively, by reading the positions of solid lines at V_b = 0 V in Figure 2b. The extracted bandgap values fall within a reasonable range for semiconducting SWNTs with diameters of ∼2.2 and ∼1.6 nm determined from AFM (Figure S2).[25−27] In addition, we can estimate that the second and third paired subbands have energy gaps of ∼0.86 and ∼1.44 eV for the top SWNT (c2 of the bottom SWNT is out of the applied bias range). We note that the extracted valence and conduction bands are not perfectly symmetric (e.g., for top SWNT in Figure 2). The separation between v2 and v3 also deviates from two times of that between v1 and v2. This behavior may be related to the trigonal warping effect and the many-body renormalization of the nanotube band structure.[8,28−30]

When the external voltages (V_{bg} and V_b) are applied to SWNTs, all the subbands shift by the amount of $\psi_{1,2}$ relative to the intrinsic Fermi energy $E_{i1,2}$ in each SWNT. We call this effect the band shift, and it is defined as $\psi_{1,2} = -(E_{F1,2} - E_{i1,2})$ (also see eq 1). Consequently, the total subband shifts are expressed to be $-eV_b + \psi_1$ for biased top SWNT and ψ_2 for the grounded bottom SWNT with $E_{F1} = -eV_b$ and E_{F2} = 0 eV. Our analysis on the experimental tunneling spectrum in Figure 2b, however, implies the band shifts ψ_1 and ψ_2 are marginal. This is because the slopes of the red and blue lines in Figure 2b are close to −1 and 0 for the biased top SWNT and grounded bottom SWNT, respectively, indicating $\psi_1 \approx 0$ eV and $\psi_2 \approx 0$ eV. The weak dependence of tunneling spectra on the backgate voltages (Figure 2c) also indicates a small band shift. To explain the small band shift effect and validate our experimental interpretation (Figure 2b), we establish a theoretical model taking into account both geometric and quantum capacitance of SWNTs (Supporting Information Note 2, Figure S6, Figure S7, Note 3).[31−34] Importantly, ψ_1 and ψ_2 show much smaller band shifts at the junction compared to those outside the junction when doped with charges carrying the same sign (Figure S7a,b and Figure S8). This originates from the strong charge repulsion at the junction, but it quickly disappears outside the junction. This result is consistent with the experimental data shown in Figure 2c, where the tunneling spectra show a rather weak dependence on the backgate voltages. We also observe that the amount of band shifts at the junction induced by V_b is small compared to the applied V_b (Figure S7c,d), which is consistent with our experimental result shown in Figure 2b. The charge repulsion effect at the junction in addition to the large quantum capacitance of SWNTs (compared to the geometric capacitance) and the low experimental gating efficiency result in the small band shifts observed in Figure 2.

We also fabricate and measure a tunneling junction composed of a metallic (bottom) and a semiconducting (top) SWNT heterojunction. The gate-dependent measure-

https://dx.doi.org/10.1021/acs.nanolett.0c02585
Nano Lett. 2020, 20, 6712−6718

ment at near zero-bias condition for each SWNT is shown in Figure S9. The diameters of the metallic and semiconducting SWNTs are about 1.2 and 2.0 nm, respectively (Figure S10). Figure 3a presents the measured dI/dV_b spectrum at $V_{bg} = -40$ V at 40 K when the top semiconducting SWNT is grounded while the bottom metallic SWNT is biased. Note that the magnitudes of the differential conductance in two heterojunctions are in the same order. The 2D differential conductance map as a function of both V_b and V_{bg} is shown in Figure S11 where a weak dependence of dI/dV_b on the backgate voltages is observed. The peaks that are assigned to the elastic band-to-band tunneling are marked by the blue arrows, which are associated with tunneling into the van Hove singularities of 1D subbands in two SWNTs. Figure 3b shows the spectrum analysis of Figure 3a in the similar manner as elaborated in Figure 2b. The solid blue lines represent the *vi* and *ci* for the grounded semiconducting SWNT, whereas those of the biased metallic SWNT are shown in the solid red lines. The slopes of the solid blue and red lines in Figure 3b and the results in Figure S11 show that the V_b- and V_{bg}-induced band shift is small. The two prominent peaks in Figure 3a at $V_b = -0.89$ and 1.04 V are attributed to the elastic band-to-band tunneling when v1 of the metallic SWNT aligns with v1 of the semiconducting SWNT and when c1 of the metallic SWNT aligns with the Fermi energy of the semiconducting SWNT, respectively. The spectrum analysis yields a separation of v1 and c1 to be ∼1.80 eV, which is a reasonable gap value for a metallic SWNT with a diameter of ∼1.2 nm.[25−27] The peaks that are not marked by blue arrows are much weaker with broader line widths than most of the marked ones. They are likely assigned to be the phonon-assisted inelastic tunneling associated with the parent elastic band-to-band tunneling peaks (marked by the blue arrows). This is because they all appear to be about 0.16∼0.2 eV above or below the marked peaks whose energy is close to the prominent phonon modes in hBN and SWNTs.[25,35] We note that the peak sitting at $V_b = -0.46$ V is not very sharp compared to other marked ones. However, there is no strong peak that can be assigned to its parent elastic tunneling peak. The extracted quasi-particle bandgap for the semiconducting SWNT is ∼0.41 eV, which is also a reasonable number given that the diameter is about 2.0 nm.[25−27]

In summary, we demonstrate a tunneling spectroscopy in the unique 1D carbon nanotube-hexagonal boron nitride-carbon nanotube heterojunctions with a greatly extended spectroscopy window (∼2 eV). We measure the tunneling current between two crossed SWNTs separated by few-layered hBN. We observe many sharp tunneling peaks at low temperature that are assigned to the elastic band-to-band tunneling associated with van Hove singularities in the 1D subbands. The measured tunneling spectra allow a determination of quasi-particle bandgaps and higher-lying subbands of the constituent SWNTs on the insulating substrate. Our experimental observation and interpretation are further supported by our theoretical model including both geometric and quantum capacitive effect. Future studies of tunneling behavior between metallic SWNTs in similar heterojunctions have the potential to reveal Luttinger liquid physics across a wide energy scale that is not currently accessible.[36]

METHODS

Preparation of Heterojunctions. SWNTs of high quality in this study were grown by the chemical vapor deposition method. Long bottom SWNTs (hundreds of μm in length) with a sparse density were directly grown on fresh hBN flakes that were exfoliated on SiO_2/Si substrates. Top SWNTs with a desirable density were grown on separate SiO_2/Si substrates. Few-layered hBN flakes (two or three layers) were exfoliated with the assistance of a step motor. A slow exfoliation speed can boost the yield of few-layered hBN with a large size. The polycarbonate (PC) polymer was used to assemble the heterojunctions because it enables a reliable pick up of few-layered hBN.[22] In the dry-transfer process, the top SWNT, few-layered hBN, and the bottom SWNT on top of a large bottom hBN substrate were sequentially picked up by PC. The typical temperatures for picking up SWNTs and few-layered hBN were about 95 and 110 °C, respectively. The release temperature for depositing the heterojunction onto a fresh SiO_2/Si (285 nm SiO_2) substrate was set at 175 °C. The PC capping on top was finally removed by chloroform.

ASSOCIATED CONTENT

Supporting Information

The Supporting Information is available free of charge at https://pubs.acs.org/doi/10.1021/acs.nanolett.0c02585.

Structural characterizations, electrical transport data, and theoretical calculation of the tunneling heterojunctions (PDF)

AUTHOR INFORMATION

Corresponding Authors

Sihan Zhao − *Department of Physics, University of California at Berkeley, Berkeley, California 94720, United States;* orcid.org/0000-0003-2162-734X; Email: sihanzhao88@berkeley.edu

Feng Wang − *Department of Physics, University of California at Berkeley, Berkeley, California 94720, United States; Materials Sciences Division, Lawrence Berkeley National Laboratory, Berkeley, California 94720, United States; Kavli Energy NanoSciences Institute at the University of California, Berkeley and the Lawrence Berkeley National Laboratory, Berkeley, California 94720, United States*; Email: fengwang76@berkeley.edu

Authors

SeokJae Yoo − *Department of Physics, University of California at Berkeley, Berkeley, California 94720, United States; Department of Physics, Korea University, Seoul 02841, Republic of Korea*

Sheng Wang − *Department of Physics, University of California at Berkeley, Berkeley, California 94720, United States; Materials Sciences Division, Lawrence Berkeley National Laboratory, Berkeley, California 94720, United States;* orcid.org/0000-0001-7923-478X

Bosai Lyu − *Key Laboratory of Artificial Structures and Quantum Control (Ministry of Education), School of Physics and Astronomy, Shanghai Jiao Tong University, Shanghai 200240, China;* orcid.org/0000-0001-8044-5509

Salman Kahn − *Department of Physics, University of California at Berkeley, Berkeley, California 94720, United States; Materials Sciences Division, Lawrence Berkeley National Laboratory, Berkeley, California 94720, United States*

Fanqi Wu − *Department of Chemical Engineering and Materials Science, University of Southern California, Los Angeles, California 90089, United States*

https://dx.doi.org/10.1021/acs.nanolett.0c02585
Nano Lett. 2020, 20, 6712−6718

Zhiyuan Zhao − *Department of Chemical Engineering and Materials Science, University of Southern California, Los Angeles, California 90089, United States*
Dingzhou Cui − *Department of Chemical Engineering and Materials Science, University of Southern California, Los Angeles, California 90089, United States*
Wenyu Zhao − *Department of Physics, University of California at Berkeley, Berkeley, California 94720, United States*
Yoseob Yoon − *Department of Physics, University of California at Berkeley, Berkeley, California 94720, United States; Materials Sciences Division, Lawrence Berkeley National Laboratory, Berkeley, California 94720, United States;* orcid.org/0000-0002-8832-897X
M. Iqbal Bakti Utama − *Department of Physics and Department of Materials Science and Engineering, University of California at Berkeley, Berkeley, California 94720, United States; Materials Sciences Division, Lawrence Berkeley National Laboratory, Berkeley, California 94720, United States;* orcid.org/0000-0002-4454-8348
Wu Shi − *Department of Physics, University of California at Berkeley, Berkeley, California 94720, United States; Materials Sciences Division, Lawrence Berkeley National Laboratory, Berkeley, California 94720, United States*
Kenji Watanabe − *Research Center for Functional Materials, National Institute for Materials Science, Tsukuba 305-0044, Japan;* orcid.org/0000-0003-3701-8119
Takashi Taniguchi − *International Center for Materials Nanoarchitectonics, National Institute for Materials Science, Tsukuba 305-0044, Japan;* orcid.org/0000-0002-1467-3105
Michael F. Crommie − *Department of Physics, University of California at Berkeley, Berkeley, California 94720, United States; Materials Sciences Division, Lawrence Berkeley National Laboratory, Berkeley, California 94720, United States; Kavli Energy NanoSciences Institute at the University of California, Berkeley and the Lawrence Berkeley National Laboratory, Berkeley, California 94720, United States;* orcid.org/0000-0001-8246-3444
Zhiwen Shi − *Key Laboratory of Artificial Structures and Quantum Control (Ministry of Education), School of Physics and Astronomy, Shanghai Jiao Tong University, Shanghai 200240, China; Collaborative Innovation Center of Advanced Microstructures, Nanjing 210093, China;* orcid.org/0000-0002-3928-2960
Chongwu Zhou − *Department of Chemical Engineering and Materials Science and Department of Electrical Engineering, University of Southern California, Los Angeles, California 90089, United States;* orcid.org/0000-0001-8448-8450

Complete contact information is available at: https://pubs.acs.org/10.1021/acs.nanolett.0c02585

Author Contributions

▲S.Z., S.Y., and S.W. contributed equally to this work.

Author Contributions

F.Wang, S.Z., and S.Y. conceived the project. F.Wang supervised the study. S.Z. transferred samples and fabricated the devices. S.Z. performed the transport measurements. S.Y established a theoretical model to interpret the experimental results. S.Y performed the numerical simulation. S.Z. also contributed to the experimental interpretation and discussed the theoretical model with S.Y. S.W. carried out the AFM scanning before and after sample transfer. S.K., W.Z., Y.Y., M.I.B.U., W.S., and M.F.C. contributed to the sample preparation. B.L., F.Wu, Z.Z, D.C., Z.S., and C.W. contributed to the nanotube growth. K.W. and T.T. provided the hBN crystals. S.Z., S.Y., and F.Wang analyzed the experimental and theoretical results and wrote the manuscript. All authors discussed the results and contributed to the manuscript preparation.

Notes

The authors declare no competing financial interest.

■ ACKNOWLEDGMENTS

The device fabrication and theoretical analysis was supported by the NSF award 1808635. The electrical measurement was supported by the Office of Naval research (MURI award N00014-16-1-2921). S.Y. was supported by the National Research Foundation of Korea (NRF) grants funded by the Ministry of Education (NRF-2017R1A6A3A11034238) and the Ministry of Science and ICT (NRF-2019R1A4A1028121 and CAMM-2014M3A6B3063710). Z.S. acknowledges support from National Natural Science Foundation of China (11774224), National Key Research and Development Program of China (2016YFA0302001), and additional support from a Shanghai talent program. F.Wu, Z.Z, D.C., and C.Z. acknowledge National Science Foundation for financial support under Grant 769 K521. K.W. and T.T. acknowledge support from the Elemental Strategy Initiative conducted by the MEXT, Japan and the CREST (JPMJCR15F3).

■ REFERENCES

(1) Kittel, C. *Introduction to Solid State Physics*, 8th ed.; Willey & Sons: New York, 2005.
(2) Luttinger, J. M. An Exactly Soluble Model of a Many-Fermion System. *J. Math. Phys.* **1963**, *4*, 1154−1162.
(3) Tomonaga, S.-i. Remarks on Bloch's Method of Sound Waves applied to Many-Fermion Problems. *Prog. Theor. Phys.* **1950**, *5*, 544−569.
(4) Haldane, F. D. M. 'Luttinger liquid theory' of one-dimensional quantum fluids. I. Properties of the Luttinger model and their extension to the general 1D interacting spinless Fermi gas. *J. Phys. C: Solid State Phys.* **1981**, *14*, 2585−2609.
(5) Giamarchi, T. *Quantum Physics in One Dimension*; Oxford University Press: New York, 2004.
(6) Odom, T. W.; Huang, J. L.; Kim, P.; Lieber, C. M. Atomic Structure and Electronic Properties of Single-Walled Carbon Nanotubes. *Nature* **1998**, *391*, 62−64.
(7) Wilder, J. W. G.; Venema, L. C.; Rinzler, A. G.; Smalley, R. E.; Dekker, C. Electronic Structure of Atomically Resolved Carbon Nanotubes. *Nature* **1998**, *391*, 59−62.
(8) Lin, H.; Lagoute, J.; Repain, V.; Chacon, C.; Girard, Y.; Lauret, J. S.; Ducastelle, F.; Loiseau, A.; Rousset, S. Many-Body Effects in Electronic Bandgaps of Carbon Nanotubes Measured by Scanning Tunnelling Spectroscopy. *Nat. Mater.* **2010**, *9*, 235−238.
(9) Bockrath, M.; Cobden, D. H.; Lu, J.; Rinzler, A. G.; Smalley, R. E.; Balents, L.; McEuen, P. L. Luttinger-Liquid Behaviour in Carbon Nanotubes. *Nature* **1999**, *397*, 598−607.
(10) Yao, Z.; Postma, H. W. C.; Balents, L.; Dekker, C. Carbon Nanotube Intramolecular Junctions. *Nature* **1999**, *402*, 273−276.
(11) Gao, B.; Komnik, A.; Egger, R.; Glattli, D. C.; Bachtold, A. Evidence for Luttinger-Liquid Behavior in Crossed Metallic Single-Wall Nanotubes. *Phys. Rev. Lett.* **2004**, *92*, 216804.
(12) Zhao, S.; Wang, S.; Wu, F.; Shi, W.; Utama, I. B.; Lyu, T.; Jiang, L.; Su, Y.; Wang, S.; Watanabe, K.; et al. Correlation of Electron Tunneling and Plasmon Propagation in a Luttinger Liquid. *Phys. Rev. Lett.* **2018**, *121*, 47702.

(13) Lee, G. H.; Yu, Y. J.; Lee, C.; Dean, C.; Shepard, K. L.; Kim, P.; Hone, J. Electron Tunneling through Atomically Flat and Ultrathin Hexagonal Boron Nitride. *Appl. Phys. Lett.* **2011**, *99*, 243114.
(14) Ahmed, F.; Heo, S.; Yang, Z.; Ali, F.; Ra, C. H.; Lee, H. I.; Taniguchi, T.; Hone, J.; Lee, B. H.; Yoo, W. J. Dielectric Dispersion and High Field Response of Multilayer Hexagonal Boron Nitride. *Adv. Funct. Mater.* **2018**, *28*, 1804235.
(15) Mishchenko, A.; Tu, J. S.; Cao, Y.; Gorbachev, R. V.; Wallbank, J. R.; Greenaway, M. T.; Morozov, V. E.; Morozov, S. V.; Zhu, M. J.; Wong, S. L.; et al. Twist-Controlled Resonant Tunnelling in Graphene/Boron Nitride/Graphene Heterostructures. *Nat. Nanotechnol.* **2014**, *9*, 808−813.
(16) Kang, S.; Fallahazad, B.; Lee, K.; Movva, H.; Kim, K.; Corbet, C. M.; Taniguchi, T.; Watanabe, K.; Colombo, L.; Register, L. F.; et al. Bilayer Graphene-Hexagonal Boron Nitride Heterostructure Negative Differential Resistance Interlayer Tunnel FET. *IEEE Electron Device Lett.* **2015**, *36*, 405−407.
(17) Zhao, Y.; Wan, Z.; Xu, X.; Patil, S. R.; Hetmaniuk, U.; Anantram, M. P. Negative Differential Resistance in Boron Nitride Graphene Heterostructures: Physical Mechanisms and Size Scaling Analysis. *Sci. Rep.* **2015**, *5*, 1−10.
(18) Kim, K.; Prasad, N.; Movva, H. C. P.; Burg, G. W.; Wang, Y.; Larentis, S.; Taniguchi, T.; Watanabe, K.; Register, L. F.; Tutuc, E. Spin-Conserving Resonant Tunneling in Twist-Controlled WSe_2 -hBN-WSe_2 Heterostructures. *Nano Lett.* **2018**, *18*, 5967−5973.
(19) Wang, Z.; Rhodes, D. A.; Watanabe, K.; Taniguchi, T.; Hone, J. C.; Shan, J.; Mak, K. F. Evidence of High-Temperature Exciton Condensation in Two-Dimensional Atomic Double Layers. *Nature* **2019**, *574*, 76−80.
(20) Appenzeller, J.; Lin, Y. M.; Knoch, J.; Avouris, P. Band-to-Band Tunneling in Carbon Nanotube Field-Effect Transistors. *Phys. Rev. Lett.* **2004**, *93*, 196805.
(21) Wang, L.; Meric, I.; Huang, P. Y.; Gao, Q.; Gao, Y.; Tran, H.; Taniguchi, T.; Watanabe, K.; Campos, L. M.; Muller, D. A.; Guo, J.; Kim, P.; Hone, J.; Shepard, K. L.; Dean, C. R. One-Dimensional Electrical Contact to a Two-Dimensional Material. *Science* **2013**, *342*, 614−617.
(22) Zomer, P. J.; Guimarães, M. H. D.; Brant, J. C.; Tombros, N.; Van Wees, B. J. Fast Pick up Technique for High Quality Heterostructures of Bilayer Graphene and Hexagonal Boron Nitride. *Appl. Phys. Lett.* **2014**, *105*, No. 013101.
(23) Chen, C. J. *Introduction to Scanning Tunneling Microscopy*; Oxford University Press: Oxford, 2007.
(24) Bardeen, J. Tunnelling from a Many-Particle Point of View. *Phys. Rev. Lett.* **1961**, *6*, 57.
(25) Saito, R.; Dresselhaus, G.; Dresselhaus, M. S. *Physical Properties of Carbon Nanotubes*; Imperial College Press: London, 1998.
(26) Jorio, A.; Araujo, P. T.; Doorn, S. K.; Maruyama, S.; Chacham, H.; Pimenta, M. A. The Kataura Plot over Broad Energy and Diameter Ranges. *Phys. Status Solidi B* **2006**, *243*, 3117−3121.
(27) Weisman, R. B.; Bachilo, S. M. Dependence of Optical Transition Energies on Structure for Single-Walled Carbon Nanotubes in Aqueous Suspension: An Empirical Kataura Plot. *Nano Lett.* **2003**, *3*, 1235−1238.
(28) Saito, R.; Dresselhaus, G.; Dresselhaus, M. Trigonal Warping Effect of Carbon Nanotubes. *Phys. Rev. B: Condens. Matter Mater. Phys.* **2000**, *61*, 2981−2990.
(29) Sato, K.; Saito, R.; Jiang, J.; Dresselhaus, G.; Dresselhaus, M. Discontinuity in the Family Pattern of Single-Wall Carbon Nanotubes. *Phys. Rev. B: Condens. Matter Mater. Phys.* **2007**, *76*, 195446.
(30) Wei, X.; Tanaka, T.; Yomogida, Y.; Sato, N.; Saito, R.; Kataura, H. Experimental Determination of Excitonic Band Structures of Single-Walled Carbon Nanotubes Using Circular Dichroism Spectra. *Nat. Commun.* **2016**, *7*, 1−9.
(31) John, D. L.; Castro, L. C.; Pulfrey, D. L. Quantum Capacitance in Nanoscale Device Modeling. *J. Appl. Phys.* **2004**, *96*, 5180−5184.
(32) Dröscher, S.; Roulleau, P.; Molitor, F.; Studerus, P.; Stampfer, C.; Ensslin, K.; Ihn, T. Quantum Capacitance and Density of States of Graphene. *Appl. Phys. Lett.* **2010**, *96*, 152104.
(33) Guo, J.; Goasguen, S.; Lundstrom, M.; Datta, S. Metal-Insulator-Semiconductor Electrostatics of Carbon Nanotubes. *Appl. Phys. Lett.* **2002**, *81*, 1486.
(34) Mintmire, J. W.; White, C. T. Universal Density of States for Carbon Nanotubes. *Phys. Rev. Lett.* **1998**, *81*, 2506.
(35) Gorbachev, R. V.; Riaz, I.; Nair, R. R.; Jalil, R.; Britnell, L.; Belle, B. D.; Hill, E. W.; Novoselov, K. S.; Watanabe, K.; Taniguchi, T.; et al. Hunting for Monolayer Boron Nitride: Optical and Raman Signatures. *Small* **2011**, *7*, 465−468.
(36) Vu, D.; Iucci, A.; Das Sarma, S. Tunneling Conductance of Long-Range Coulomb Interacting Luttinger Liquid. *Phys. Rev. Research* **2020**, *2*, 1.

https://dx.doi.org/10.1021/acs.nanolett.0c02585
Nano Lett. 2020, 20, 6712−6718